ARTICLE OPEN

Improving stability of organometallic-halide perovskite solar cells using exfoliation two-dimensional molybdenum chalcogenides

Meiying Liang [1]✉, Adnan Ali [2], Abdelhak Belaidi [2], Mohammad Istiaque Hossain[2], Oskar Ronan[1], Clive Downing[1], Nouar Tabet [3], Stefano Sanvito[1], Fedwa El-Mellouhi[2]✉ and Valeria Nicolosi [1]✉

Organometallic-halide perovskite solar cells (PSCs) are emerging as the most promising next generation solar cell devices. However, the stability is still the main bottleneck of their further development. Here, we introduce two-dimensional (2D) molybdenum chalcogenides (MoS_2 and $MoSe_2$) (MCs) nanoflakes as a buffer layer between perovskite layer and hole transport layer (HTL) to improve the stability of the organometallic-halide PSCs. 2D MCs are obtained via liquid-phase exfoliated (LPE) approach, and Glass/ FTO/compact-TiO_2/ mesoporous-TiO_2/$FA_{85}MA_{15}PbI_{85}Br_{15}$/2D MCs/Spiro-OMeTAD/Au structured solar cell devices are designed and fabricated. In this system, 2D MCs act both as a protective layer and an additional HTL of PSCs. This kind of PSCs achieve a relatively high-power conversion efficiency (PCE) of 14.9%, along with a much longer lifetime stability compared to the standard PSCs. After 1 h, PCE of the PSC adding a 2D MCs buffer layer could maintain 93.1% of initial value, while the PCE of the standard PSC dropped dramatically to 78.2% of initial efficiency. Our results pave the way towards the implementation of 2D MCs nanoflakes as a material able to boost the shelf life of PSCs and further provide the opportunity to fabricate large-area PSCs in view of their commercialization.

INTRODUCTION

Traditional solar energy conversion devices based on crystalline silicon face the challenge of resource limitations and their energy intensive production process[1]. Therefore, there is an urgent need to develop cheap and efficient solar cells[2,3]. High-performance, economically viable, abundant and scalable device components are key to developing the solar cell materials. Organometallic-halide perovskite solar cells (PSCs) are among of the most promising candidates for next generation solar cell technology[4–6]. Organometallic-halide perovskite have intense light absorption coefficient ($1.5 \times 10^4 \, cm^{-1}$ at 550 nm), long electron and hole diffusion length (up to 1 mm) and high carrier mobility (1–$10 \, cm^2 \, V^{-1} \, s^{-1}$)[7–10]. However, the stability of PSCs has become a major barrier for their further development in the market[11–17]. Because perovskites are very sensitive to environment such as air, UV light, water, thermal stress and other factors[18–20]. Normally, adding hole and electron transporting layers (HTL and ETL, respectively) in PSCs between the perovskite layer and the electrodes helps to separate and selectively collect the generated charge carriers (holes at the cathode and electrons at the anode electrode)[21]. To date, TiO_2 is the most widely used ETL material for PSCs to prevent electron-hole recombination at the anode[4,6,22]. This kind of ETL typically consists of compact TiO_2 layer (c-TiO_2, 50–80 nm) and mesoporous TiO_2 layer (mp-TiO_2, 200–300 nm)[4,6,22]. On the other hand, 2,2′,7,7′-tetrakis-(N,N-di-4-methoxyphenylamino)-9,9′-spiro-bifluorene (Spiro-MeOTAD) represents the reference hole transport material (HTM) used for PSCs due to its facile deposition and high performance[23]. It could effectively transfer the photogenerated holes from the perovskite to the cathode while blocking the electrons from reaching the cathode. Unfortunately, Spiro-

OMeTAD also has serious degradation issues induced by UV light, temperature, additives, and environmental conditions[23]. It appears that Spiro-OMeTAD HTL contributes to the poor stability of PSCs solar cell devices as well. Therefore, many other HTMs, such as copper (I) thiocyanate (CuSCN)[24], nickel (II) oxide (NiO)[25], and poly (3,4-ethylenedioxythiophene) polystyrene sulfonate (PEDOT: PSS)[26,27], have been explored to improve the PV performance including the stability of PSCs. However, these alternative HTMs could hardly compete to replace the ideal band edge positions of the Spiro-OMeTAD with respect to the perovskite absorbing layer. Another strategy to improve the stability of PSCs is inserting a buffer layer into the device structure to optimize the interface between the perovskite layer and Spiro-OMeTAD HTL[28–31].

For either a HTL or a buffer layer, two-dimensional (2D) molybdenum chalcogenides (MCs) (such as molybdenum disulfide [MoS_2] and molybdenum diselenide [$MoSe_2$]) are emerging as potential candidates due to their high carrier mobility, low cost (e.g. MoS_2 Sigma-Aldrich, 0.85 € g^{-1}), and solution-processable properties[29–36]. 2D MoS_2 nanoflakes have improved the efficient charge extraction across the HTL reducing recombination at the interfaces[35,36]. Therefore, combination of 2D MCs and perovskite gives us opportunity to obtain solar cells with good efficiency and longer-term stability.

In this work, 2D MCs (such as MoS_2 and $MoSe_2$) nanoflakes were prepared via liquid-phase exfoliation (LPE) approach, which is a non-destructive, insensitive (to the environment such as air and water) and solution-processable method[37,38]. Then, these 2D MCs nanoflakes were utilized as a buffer layer material between perovskite layer and HTL (i.e., Spiro-OMeTAD) of the device to enhance the stability of PSCs. Based on the previous studies,

[1]School of Chemistry, Centre for Research on Adaptive Nanostructures and Nanodevices (CRANN) and Advanced Materials and BioEngineering Research (AMBER), Trinity College Dublin, Dublin 2, Ireland. [2]Qatar Environment and Energy Research Institution (QEERI), Hamad Bin Khalifa University (HBKU), Doha 34110, Qatar. [3]Department of Applied Physics and Astronomy, University of Sharjah, P. O. Box 27272, Sharjah, UAE. ✉email: liangm@tcd.ie; felmellouhi@hbku.edu.qa; nicolov@tcd.ie
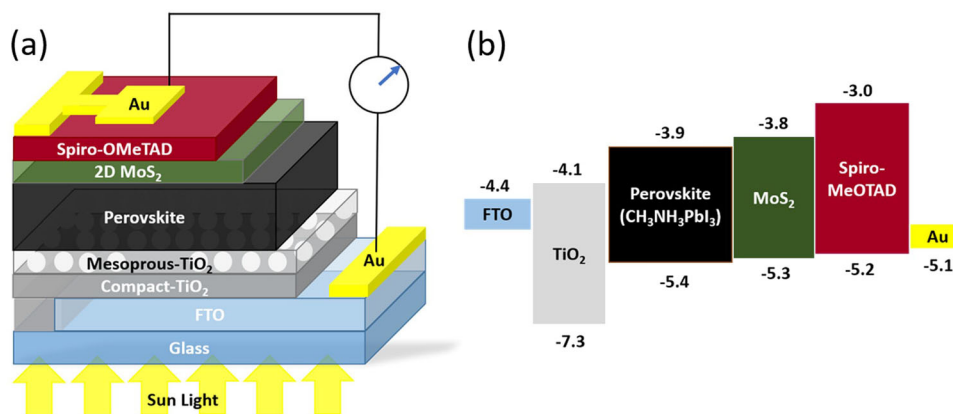
Fig. 1 Structure of the perovskite solar adding a 2D MoS₂ HTL buffer layer. a Sketch of the perovskite based solar cell illustrating the applied 2D MoS₂ nanoflakes as a buffer layer between perovskite and Spiro-OMeTAD of PSCs. **b** Band energy diagram of the whole structure.
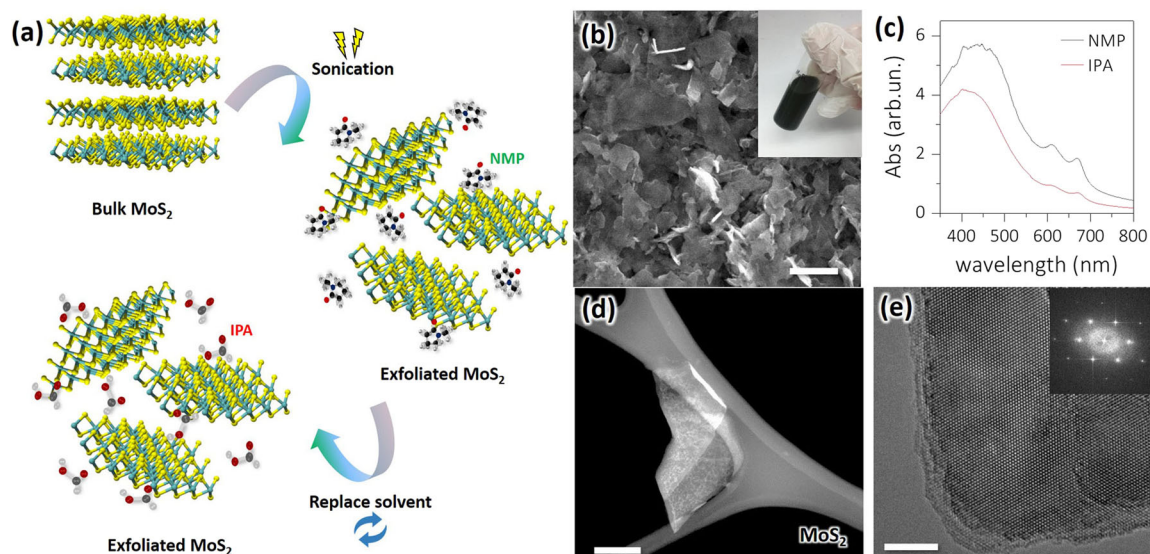

Fig. 2 Preparation of the 2D MoS₂ nanosheets. a Scheme of the preparation of 2D MoS₂ nanoflakes using LPE approach. **b** SEM image of exfoliated 2D MoS₂ nanoflakes, and inside are exfoliated MoS₂ dispersions in an IPA (Scale bar is 500 nm). **c** Absorbance spectra of exfoliated MoS₂ nanoflakes in NMP and IPA solvents, respectively. **d** HAADF-STEM (Scale bar is 100 nm) and **e** high-resolution TEM images of exfoliated MoS₂, inset in part **e** is fast Fourier transform pattern of exfoliated MoS₂ (Scale bar is 5 nm).

Glass/FTO/compact-TiO₂/mesoporous-TiO₂/$FA_{85}MA_{15}PbI_{85}Br_{15}$/2D MCs/Spiro-OMeTAD/Au structured solar cells were designed and demonstrated. (a sketch of the solar cell and its band energy diagram is shown in Fig. 1a and b)[22,29,31,39]. We investigated various preparation conditions of 2D MC HTL buffer layers followed with a characterization of the devices' power conversion efficiency (PCE) and stability.

RESULTS

Preparation of 2D MCs

2D MCs nanoflakes (i.e., MoS₂ and MoSe₂) were obtained *via* sonication-assisted LPE approach. The principle of LPE method is quite simple. Because of the characteristic of layered structured materials (i.e., strong chemical bonds in-plane but weak interaction out-of-plane), ultrasonic energy can easily break up weak van der Waals interactions between each layer to obtain exfoliated 2D nanoflakes. As shown in Fig. 2a, taking MoS₂ as an example, first, bulk MoS₂ was exfoliated in N-Methyl-2-pyrrolidone (NMP), whose Hansen solubility parameters and surface energy are suitable for most 2D layered materials, using a probe sonic tip[37]. The sonic tip

was pulsed for 6 s on and 2 s off with 60% amplitude of power to avoid damage to the processor and reduce solvent heating, and thus, degradation. During sonication, the temperature of the system was cooled to around 5 °C by continuous flow of cooling water. Once sonicated, the dispersion was subjected to centrifugation to remove any unexfoliated materials. Then, the top 60% supernatant was collected. However, although NMP is the most effective solvent for the MoS₂ exfoliation, it is toxic (Health code ≥ 2, NFPA 704) and has a high boiling point (202 °C). Moreover, it dissolves the perovskite crystals during the processing. Therefore, exfoliated MoS₂ nanoflakes were transferred from NMP to isopropanol (IPA, Health code 1; NFPA 704, boiling point: 82.6 °C), forming environmentally friendly colloidal solutions (inset of Fig. 2b) with concentration up to 3 mg mL⁻¹. As shown in Fig. 2c, UV–vis spectra of exfoliated MoS₂ nanoflakes in NMP and IPA dispersions show typical feature absorption peaks of MoS₂ (one absorption peak onset about 450 nm and two peaks at around 674 nm and at around 612 nm), however, at the cost of concentration compared to they in NMP dispersion[37,40]. In addition, scanning electron microscopy (SEM, Fig. 2b) image confirms the efficient exfoliation into few-layered MoS₂
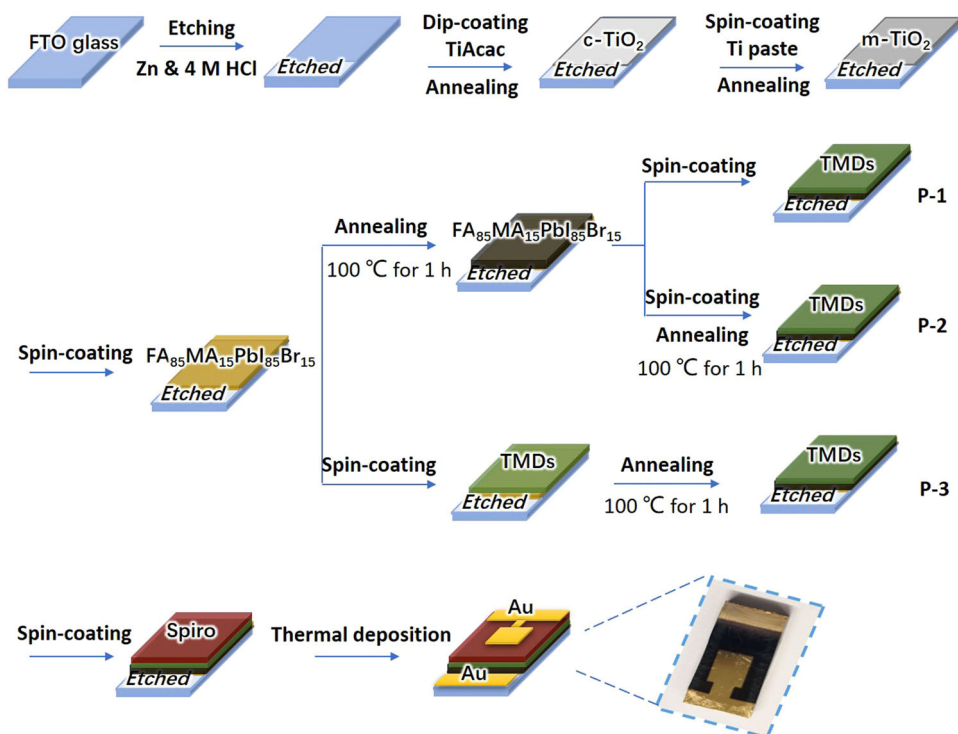
Fig. 3 Three different methods to fabricate the PSCs with a 2D MCs buffer layer. (P-1) MoS$_2$ deposited on annealed perovskite without further annealing, (P-2) MoS$_2$ is deposited on annealed perovskite film and further annealed at 100 °C for 1 h in the glove box, (P-3) MoS$_2$ is deposited on as deposited perovskite film then both films are annealed at 100 °C for 1 h.

nanoflakes. High-angle annular dark-field scanning transmission electron microscopy (HAADF-STEM, Fig. 2d) image indicates plenty of exfoliated flakes with well-defined edges and no apparent damage in the basal planes, suggesting the exfoliated material is of high quality. This is further verified by high-resolution TEM (HRTEM, Fig. 2e) and its corresponding fast Fourier transform (FFT, inset of Fig. 2e) pattern of exfoliated MoS$_2$ nanoflakes reveal the highly crystalline structure of the exfoliated MoS$_2$ nanoflakes. 2D MoSe$_2$ nanoflakes were prepared *via* the same process as MoS$_2$. HAADF-STEM, HRTEM and its corresponding FFT pattern of exfoliated 2D MoSe$_2$ nanoflakes presented in Supplementary Fig. 1a, b. Furthermore, different size of 2D MC nanoflakes obtained by centrifuging dispersions at different spin rates (1000 rpm, 3000 rpm, and 5000 rpm) called size selection. According to their TEM images and corresponding size distribution histogram (Supplementary Fig. 2a-f), we could know that when the centrifuging rate increased from 1000 rpm to 5000 rpm, the average size of the exfoliated 2D MCs nanoflakes decreased from 248.27 nm to 42.61 nm. This is expected that increasing the centrifuging rates decreased the size of the MCs nanoflakes. And the thickness of liquid-phase exfoliated 2D MC nanosheets relates to their size[37]. The relationship between the dispersed concentration, C, and mean flake dimensions for exfoliated 2D nanosheets is

$$C \propto (w \cdot t)/L^2 \tag{1}$$

where L is the length, w is the width and t is the thickness. This implies that reducing the concentration and size by increasing the centrifugation speed will result in thinner nanosheets.

Fabrication of PSCs with a 2D MCs buffer layer
As shown in Fig. 1, a 2D MCs buffer layer was added between the perovskite layer and Spiro-OMeTAD layer (so called "HTL buffer") to comprise a Glass/FTO/compact-TiO$_2$/mesoporous-TiO$_2$/FA$_{85}$MA$_{15}$PbI$_{85}$Br$_{15}$/2D MCs/Spiro-OMeTAD/Au structured PSC. As representative member of 2D MCs family, MoS$_2$, MoSe$_2$, and

MoTe$_2$ were simulated as HTL buffer layer of the same structured PSCs. As calculated (Supplementary Fig. 3a, d), adding p-type MoS$_2$, MoSe$_2$, and MoTe$_2$ show the improvement in performance due to the increase of the absorbing volume within the MC layers and improve of short-circuit current density (J$_{sc}$), Fig. 3 presents the fabrication process of the PSCs adding a 2D MCs HTL buffer. Cleaning and depositing ETL layer was done in air atmosphere, after that, samples were transferred into a glovebox to deposit the perovskite, 2D MC buffer, and Spiro-OMeTAD layers. The 2D MC nanoflakes in IPA dispersion was dropped onto the perovskite layer immediately with the spin-coating started at 2000 rpm and lasted one minute. Compared to the standard PSC, PSCs adding a MoS$_2$ HTL buffer layer, or MoSe$_2$ HTL buffer layer reduced the efficiency to some extent (Supplementary Fig. 4) and this is mainly caused by the sacrifice of the FF (Supplementary Table 1) because of the solvent (i.e., IPA) existing in 2D MCs dispersions. However, this factor could be improved by optimizing deposition process. As shown in Fig. 3, three different conditions were investigated: (P-1) MoS$_2$ deposited on annealed perovskite without further annealing; (P-2) MoS$_2$ is deposited on annealed perovskite film and further annealed at 100 °C in the glove box; (P-3) MoS$_2$ is deposited on as deposited perovskite film then both films are annealed at 100 °C. Supplementary Fig. 5a, b show the cross-section TEM images presenting the different components of the solar cell device from the front contact (FTO) to the back contact (Au) of the standard PSC and the PSC with a 2D MoS$_2$ HTL buffer layer prepared by (P-1), (P-2), and (P-3) methods, respectively. Comparing to the standard solar cell, the perovskite layer of the solar cell spin-coated the 2D MoS$_2$ dispersion by (P-1) process obviously damaged. This is because the small amount IPA solvent in 2D MoS$_2$ dispersions could induce degradation of the perovskite layer. Therefore, adding an annealing process (P-2 and P-3) could reduce the damage of IPA on the perovskite layer. However, as shown in Supplementary Fig. 5c, d, the interface between ETL and the perovskite layer of the PSC with a MoS$_2$ HTL

buffer layer annealed separately from the perovskite layer (P-2) is much smoother than the one with a MoS_2 HTL buffer layer annealed together with the perovskite layer (P-3). It implies a MoS_2 could influence the growth of the perovskite, so it can reduce the quality of the perovskite layer. Therefore, it's better to do the deposition of the MoS_2 layer onto the complete perovskite layer by (P-2) method. Figure 4 shows the cross-section TEM image of the PSC with a 2D MoS_2 HTL buffer layer prepared by (P-2) approach. It shows less roughness then expected at interfaces perovskite / 2D MoS_2 / Spiro-OMeTAD which indicates that the inclusion of the MoS_2 layer between the perovskite and the Spiro-OMeTAD did not engender big cracks. This could be seen as a good sign for the solar cell operation.

PV performance of PSCs with additional 2D MCs buffer layer
Figure 5e shows the IV curves of the four devices including standard PSC (without HTL buffer) and PSCs with a 2D MoS_2 buffer layer prepared by three different approaches as described above.
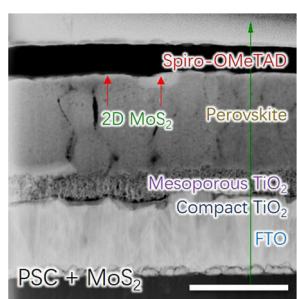

Fig. 4 TEM characterization of a PSC adding a 2D MoS_2 nanoflakes HTL buffer layer. The cross-section TEM image of a PSC adding a 2D MoS_2 nanoflakes HTL buffer layer prepared by P-2 (Scale bar is 1 μm).

It is clear that the device prepared with sequential annealing (P-2) performs as good as the standard PCS, while the PCS prepared without annealing of MoS_2 (P-1) or annealing MoS_2 together with pristine perovskite film (P-3) performed less efficiently. Interestingly, the fill factor (FF) was strongly affected (45.9% instead of 64.2%, Fig. 5c, f), followed by the open-circuit voltage (V_{oc}) (0.92 V instead of 1.01 V, Fig. 5a, f) but the short-circuit current density (J_{sc}) was only slightly affected (21.64 mA cm^{-2} instead of 22.22 mA cm^{-2}, Fig. 5b, f). This indicates that there are serious interface issues under these two preparation conditions (P-1 and P-3). It is worth noting that IPA can partially dissolve the perovskite, so adding 2D MoS_2 buffer layers may lead to a damage of the surface of perovskite and this damage can be more serious in cases of (P-1) and (P-3). In (P-1) because the 2D MoS_2 film is not annealed so the residues of IPA will have more time to get in contact with the perovskite surface. In case of (P-3), the 2D MoS_2 film is added on the as deposited perovskite film so not in form of grains (crystals) which is make it surface more soluble than in the crystalline case. This could be the reason behind the low fill factor of the solar cell devices prepared under these conditions. This is in good agreement with the cross-section TEM images as mentioned before (Supplementary Fig. 5c, d). It is worth noting that compared to a standard PSC, a PSC with a MoS_2 (P-2) layer has slightly higher V_{oc} and J_{sc} so that the efficiency of the device could maintain at 14.9% (Fig. 4d, f). This could be attributed to conducting MoS_2 nanoflakes improved charge transport property of the device[36]. What's more, it is clear from the energy band alignment (Fig. 1b) that MoS_2 can act as an electron blocking layer, which suppresses interfacial charge recombination[36]. In addition, using 2D $MoSe_2$ nanoflakes we studied the effect of the nanoflake's size to devices' PV performances. According to the IV curves (Supplementary Fig. 6a–d), we could see that smaller size gave the better PV performance due its higher J_{sc} and FF than the larger size nanoflakes. Therefore, the remaining of this manuscript focuses on small size 2D MCs nanoflakes integrated into PSC.
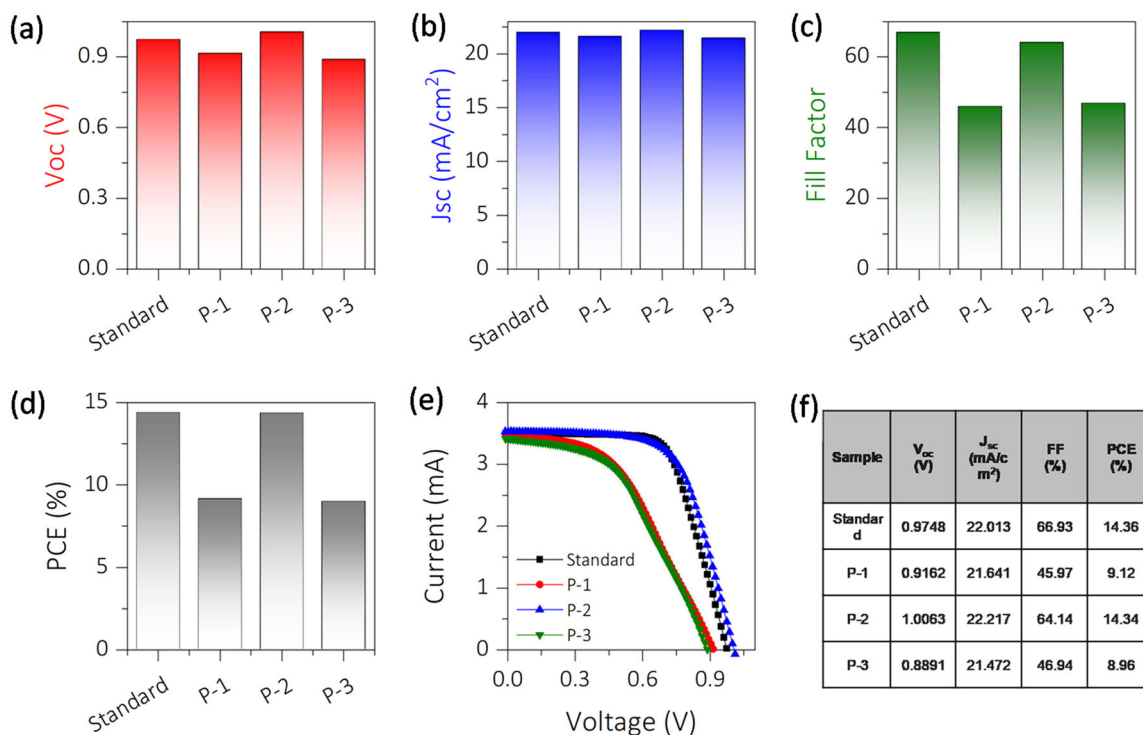

Sample	V_{oc} (V)	J_{sc} (mA/cm²)	FF (%)	PCE (%)
Standard	0.9748	22.013	66.93	14.36
P-1	0.9162	21.641	45.97	9.12
P-2	1.0063	22.217	64.14	14.34
P-3	0.8891	21.472	46.94	8.96

Fig. 5 Variation of PSC parameters of a standard PSC and a PSCs with a 2D MoS_2 HTL buffer layer prepared by P-1, P-2, and P-3 methods. **a** V_{oc}, **b** J_{sc}, **c** FF, **d** PCE, **e** IV curves, and **f** summary of V_{oc}, FF, J_{sc} and PEC values of a standard PSC and PSCs adding 2D MCs nanoflakes as P-1, P-2, and P-3.
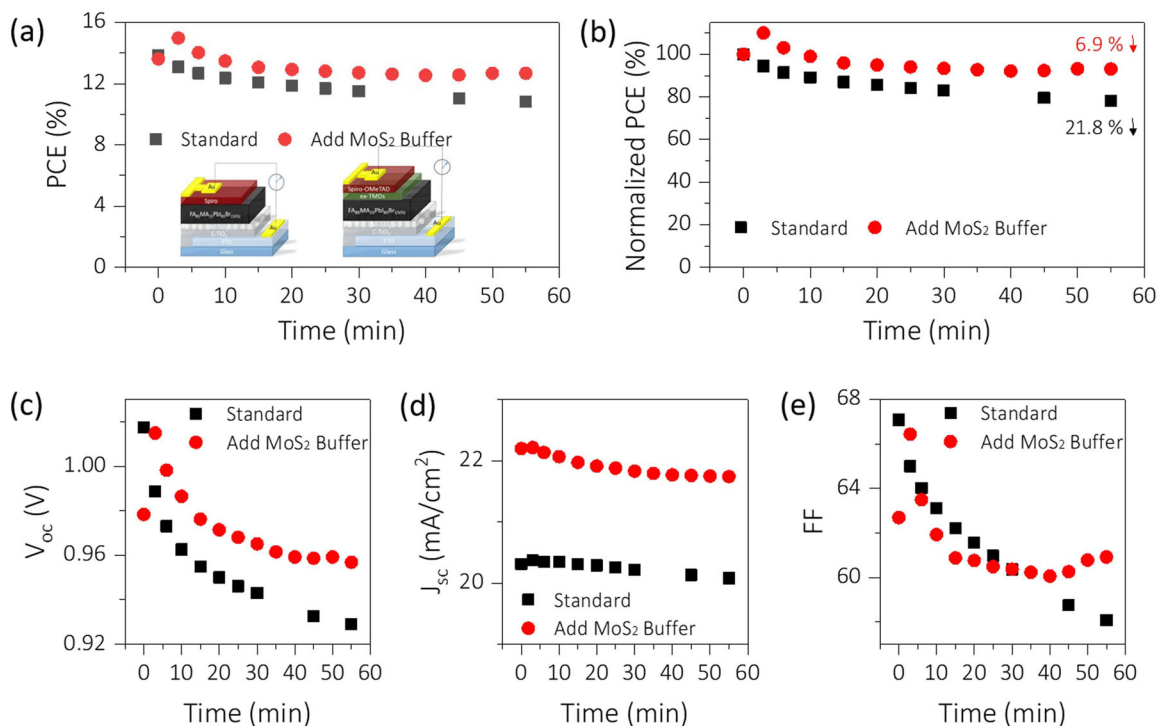
Fig. 6 Stability of the PCSs with and without a MoS$_2$ buffer layer. a PCE, **b** normalized PCE, **c** V_{oc}, **d** J_{sc}, and **e** FF of PSCs with and without a MoS$_2$ buffer layer.

Stability of PSCs with additional 2D MCs buffer layer

Dark storage studies (ISOS-D),[57] which estimated a cell's shelf life under ambient conditions when it is not exposed to light were conducted at room temperature (23 ± 4 °C) in ambient air and humidity using sun simulator (AM1.5 G including UV). PCE of the standard PSC, PSC with a 2D MoS$_2$ HTL buffer layer obtained by (P-2) and (p-3) were measured after 1 day, 1 week and 3 weeks. All PSCs were stored in ambient air at room temperature in dark. It is known that the PCE of a standard PSC using Spiro-OMeTAD as a HTL increases after several days because of the oxidation of Spiro-OMeTAD[23]. We observed the same behavior for our PSCs with/without a 2D MoS$_2$ HTL buffer layer. Interestingly, we observed that the efficiencies of these solar cells continue to increase even after 3 weeks as it is shown in Supplementary Fig. 7a-d and Supplementary Table 2. It indicates that the insertion of the MoS$_2$ layer does not have a negative effect on the aging of the PSCs devices and our PSCs are relatively stable.

What's more, we also tested the stability of PSCs with/without a 2D MoS$_2$ HTL buffer layer under continuous sun illumination (AM1.5 G including UV) in ambient air at room temperature for 1 h. As shown in Fig. 6a, the PCE of the standard PSC reached its lifetime (21.8% of its initial efficiency) in 60 min. However, the PSC with a 2D MoS$_2$ HTL buffer layer only loses 6.9% of PCE after 60 min. This result shows clearly that the 2D MoS$_2$ prepared by exfoliation and inserted as a HTL buffer is able to enhance the stability of the PSC devices. When looking at the variation of each solar cell parameter V_{oc}, J_{sc} and FF with the illuminated time, one could observe a gradual decrease of the values of these parameters with the time. However, in comparison to the standard PSC, the main difference is in the decay of the FF and J_{sc} with time, which is more pronounced in the absence of 2D MoS$_2$. This is because the 2D MoS$_2$ buffer layer can cause changes in conductivity, transparency, structure, and/or band alignment with other layers of PSCs[29,30,36,41–43]. This would result in preventing drastically changes of FF, likely by reducing recombination losses at the interface through blocking electron and accelerating charge
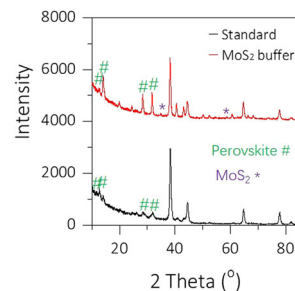

Fig. 7 XRD characterization of a PSC with/without 2D MoS$_2$ buffer layer after stability tests. XRD spectra of a standard PSC and a PSC adding an additional 2D MoS$_2$ buffer layer after stability tests under continuous sun illumination for 1h (characteristic peaks of the perovskite marked as # and MoS$_2$ marked as *, respectively).

transport, simultaneously[12,15]. In addition, the improvement of the stability also attributed to the stabilization of J_{sc}. which is related with the improved charge transfer efficiency.

In addition, IV curves of forward and backward scans for a standard PSC and a PSC adding a 2D MoS$_2$ HTL buffer layer are shown in Supplementary Fig. 8a, b. No appreciable difference was observed between backward and forward scans for the standard PSC (Supplementary Fig. 8a), while J_{sc} increased apparently leading to the increase of PCE for the PSC adding MoS$_2$ buffer layer (Supplementary Fig. 8b). This is because of improvement of the charge transport property by adding a conducting 2D MoS$_2$ HTL buffer layer between the perovskite and Spiro-OMeTAD. It also supports the conclusion that adding a 2D MoS$_2$ HTL buffer layer gives better stability than a standard PSC. X-ray diffraction (XRD) tests of a standard PSC and a PSC adding an additional 2D MoS$_2$ HTL buffer layer after stability test (working under continuously sun illumination for 1 h at room temperature in ambient air) were conducted to see the structure degradation of the perovskite layer, respectively. As shown in Fig. 7, perovskite

characteristic peaks of a PSC with a MoS$_2$ buffer layer much stronger than a standard one. It implies less degradation of the perovskite in the PSC with a 2D MoS$_2$ HTL buffer layer[36,44]. What's more, according to the energy-dispersive X-ray spectroscopy (EDX) mapping of the PSC with a 2D MoS$_2$ HTL buffer layer after IV measurement, it's apparent that a 2D MoS$_2$ HTL buffer layer efficiently prevents migration of lead (Pb), iodine (I), and bromide (Br) from the perovskite layer to the Spiro-OMeTAD HTL (Supplementary Fig. 9). In the meanwhile, a 2D MoS$_2$ HTL buffer layer also prevents the migration of metals (i.e., Au) from electrode to the Spiro-OMeTAD layer to the perovskite layer (Supplementary Fig. 9).The migration of metal through the HTL can lead to high recombination losses, which in turn cause reduction of FF and V$_{oc}$ during the operation[12,15,29].

DISCUSSION

Here, we demonstrated the use of 2D MCs nanoflakes (mainly focus on MoS$_2$) as a HTL buffer layer of PSCs (Glass/FTO/compact-TiO$_2$/mesoporous-TiO$_2$/FA$_{85}$MA$_{15}$PbI$_{85}$Br$_{15}$/2D MC/Spiro-OMeTAD/Au). Guided by our computational simulation of the device performance, we reveal that inserting suitable 2D MCs HTL buffer results in better interface quality, absorption of photon energy, and improving the stability by working as a scaffolding layer between perovskite and HTL in PSCs. 2D MCs nanoflakes are obtained via sonication-assisted LPE approach. Then, these exfoliated 2D MCs in IPA dispersions are spin-coated onto the perovskite layer and immediately annealed to remove IPA solvent to obtain the 2D MCs HTL buffer layer. Interestingly, when a 2D MCs buffer layer is added between the perovskite layer and HTL (Spiro-OMeTAD), the stability of the PSC improved apparently. PCE of the standard PSC dropped to 78.2% of original value after endurance test of 1 h under solar simulator (AM1.5 G including UV) illumination in ambient air at room temperature. However, PCE of the PSC adding a 2D MoS$_2$ HTL buffer layer could maintain 93.1% of PCE after 1 h under continuously illumination. Forward and backward IV scans and XRD, and EDX measurements of PSCs with/without a 2D MoS$_2$ HTL buffer layer support the conclusion that adding a 2D MoS$_2$ HTL buffer layer into the PSCs structure could efficiently enhance the stability of them. However, further investigations are underway to deeply understand the reasons behind this stability enhancement using prolonged tests followed by analytical experiments such as XPS and time-of-flight SIMS.

METHODS

Preparation of 2D molybdenum chalcogenides nanoflakes

Here, a typical methodology for the preparation of an exfoliated 2D molybdenum chalcogenides dispersion is described. For MoS$_2$ as an example, in the initial MoS$_2$ experiments, 4 g of MoS$_2$ powder were added to 80 mL of NMP, and a probe sonic tip was utilized to sonicate the solution for a certain number of hours (power: 60% amplitude). The sonic tip was pulsed for 6 s on and 2 s off to avoid damage to the processor and reduce solvent heating, and thus, degradation. The beaker was connected to a cooling system that allowed for cold water (5 °C) to flow around the dispersion during sonication. Then, exfoliated MoS$_2$ nanoflakes in NMP solvent were centrifuged at high spin rate (10,000 rpm) to obtain the MoS$_2$ nanoflakes. Then, these MoS$_2$ nanoflakes were redispersed in IPA through bath sonication, so exfoliated molybdenum chalcogenides nanoflakes dispersion in IPA were obtained. Afterwards, they were then centrifuged at different centrifugation rates (1000 rpm, 3000 rpm, and 5000 rpm) for 1 h, and the supernatant was retained (size selection of MoS$_2$). The same methodology was used to obtain the exfoliated MoSe$_2$ dispersions.

Fabrication of perovskite solar cells

Substrate and ETL preparation: Solar cells were fabricated on FTO glass substrates with a sheet resistance of ~8 Ω sq^{-1}. The impurities were removed from the FTO-coated substrate via a three-step cleaning process (soapy water, deionized (DI) water and isopropanol (IPA) for 15 min each).

The back side of the FTO glasses were covered with tapes. One side of the FTO glasses were etched using zinc power and 4 M HCl solution. Then, compact TiO$_2$ layer was deposited on FTO via dip-coating twice and annealing at 200 °C for 10 min and 450 °C for 30 min, respectively[39]. A precursor dip-coating solution was prepared by mixing 6 mL of titanium diisopropoxidebis(acetylacetonate) (TiAcac) solution with 54 mL of IPA. Then, mesoporous TiO$_2$ layer was deposited by spin coating for 20 s at 4000 rpm with a ramp of 2000 rpm s^{-1}, using 30 nm particle Ti paste (mixed titaniumoxide paste [Dyesol 30 NR-D] and ethanol with the ratio of 150 mg: 1 mL). After the spin-coating, the substrates were immediately annealed in a hot plate.

Perovskite precursor solution and film preparation: The perovskite solution was prepared first. Typically, 1.1 mM (508 mg mL^{-1}) of PbI$_2$, 0.183 mM (67.1 mg) of PbBr$_2$, 1.05 mM (180.5 mg) of FAI, and 0.183 mM (20.4 mg) of MABr were dissolved into a mixture of DMF: DMSO (800 μL: 200 μL) solvent. Then, the perovskite solution was spin coated in a two-step program at 1000 and 4000 rpm for 10 and 30 s, respectively. During the second step, 300 μL of chlorobenzene was poured onto the spinning substrate 20 s prior the end of the program to smooth the film. Finally, the substrate was annealed at 100 °C for 1 h in nitrogen-filled glove box.

Preparation of the 2D molybdenum chalcogenides buffer layer: Three different approaches were tried to prepare the 2D TMD buffer layer. First method is spin coating the 2D TMD layer at 2000 rpm for 20 s without any other treatment. Second and third methods added the heat treatment (100 °C for 1 h) after spin coating the 2D TMD dispersion onto the substrate. In the second method, the TMD layer was spin coated and annealed after annealing the perovskite layer at 100 °C for 1 h. But in the third method, the TMD layer was annealed together with the perovskite layer at 100 °C for 1 h.

HTL and top electrode preparation: After the deposition of the a 2D molybdenum chalcogenides buffer layer, a spirofluorene-linked methoxy triphenylamines (Spiro-OMeTAD, from Sigma-Aldrich) solution (70 mM in chlorobenzene) was spun at 4000 rpm. for 20 s. The Spiro-OMeTAD was doped with bis(trifluoromethylsulfonyl)imide lithium salt (Li-TFSI, from Sigma-Aldrich), tris(2-(1H-pyrazol-1-yl)-4-tert-butylpyridine)- cobalt(III) tris (bis(trifluoromethylsulfonyl)imide) (FK209, from Sigma-Aldrich) and 4-tert-Butylpyridine (TBP, from Sigma-Aldrich)[45–47]. The molar ratio of additives for Spiro-OMeTAD was: 0.5, 0.03 and 3.3 for Li-TFSI, FK209 and TBP, respectively. Finally, around 20 nm of gold top electrode was thermally evaporated under high vacuum.

Materials and devices characterization

Characterization of 2D MCs nanosheets: The SEM images of all samples were acquired on a Zeiss Ultra Plus (Carl Zeiss, Germany) with an acceleration voltage of 2 keV. The TEM images of exfoliated 2D MCs nanosheets were performed on a FEI Titan at 300 kV (FEI, USA). Prior to the TEM study, the nanosheet dispersion was drop-casted onto holey carbon grids (Agar Scientific, UK). The UV-vis of 2D MCs dispersion was carried out with a Cary Varian 5000i UV-vis-NIR spectrometer. The dispersion was diluted to 1:10 in ethanol/water (60:40).

Characterization of PSCs: The numerical analysis has been carried out using 1D-solar cell capacitance simulator (SCAPS-1D) software. The computations were carried out using material parameters that were extracted from relevant literatures[48–50]. During the simulation, 2D MCs materials have been used as layered structured to mimic the real device structures. The highest reported electron mobility of MoS$_2$ is 200 cm^2 V^{-1} s^{-1}[40,42]. However, the layered structure of these materials induces an anisotropy of the carrier transport. The electron mobility within the layers is excellent but it is much lower across the layers. In our device simulation, we have considered the effective mobility of 50 cm^2 V^{-1} s^{-1} as a typical mobility value based on at least two experimentally reported mobilities for MoS$_2$ layer having thickness varying from 1–23 mono-layers[51,52]. FIB-TEM technique was used to get the cross-section TEM image and EDX mapping of the PSCs. XRD measurements were performed by means of Rigaku SmartLab X-Ray Diffractometer operating at room temperature. Current-voltage (I-V) tests were conducted using Newport Corporation IV tester under sun simulator (AM1.5G including UV).

DATA AVAILABILITY

REFERENCES

1. Jean, J., Brown, P. R., Jaffe, R. L., Buonassisi, T. & Bulović, V. Pathways for solar photovoltaics. *Energy Environ. Sci.* **8**, 1200–1219 (2015).
2. Polman, A., Knight, M., Garnett, E. C., Ehrler, B. & Sinke, W. C. Photovoltaic materials: present efficiencies and future challenges. *Science* **352**, aad4424 (2016).
3. Sivula, K. & van de Krol, R. Semiconducting materials for photoelectrochemical energy conversion. *Nat. Rev. Mater.* **1**, 15010 (2016).
4. Burschka, J. et al. Sequential deposition as a route to high-performance perovskite-sensitized solar cells. *Nature* **499**, 316 (2013).
5. Jeon, N. J. et al. Compositional engineering of perovskite materials for high-performance solar cells. *Nature* **517**, 476 (2015).
6. Liu, M., Johnston, M. B. & Snaith, H. J. Efficient planar heterojunction perovskite solar cells by vapour deposition. *Nature* **501**, 395 (2013).
7. Green, M. A., Ho-Baillie, A. & Snaith, H. J. The emergence of perovskite solar cells. *Nat. Photonics* **8**, 506 (2014).
8. Kojima, A., Teshima, K., Shirai, Y. & Miyasaka, T. Organometal halide perovskites as visible-light sensitizers for photovoltaic cells. *J. Am. Chem. Soc.* **131**, 6050–6051 (2009).
9. Motta, C., El-Mellouhi, F. & Sanvito, S. Charge carrier mobility in hybrid halide perovskites. *Sci. Rep.* **5**, 12746 (2015).
10. Wojciechowski, K., Saliba, M., Leijtens, T., Abate, A. & Snaith, H. J. Sub-150 °C processed meso-superstructured perovskite solar cells with enhanced efficiency. *Energy Environ. Sci.* **7**, 1142–1147 (2014).
11. Ava, T. T., Al Mamun, A., Marsillac, S. & Namkoong, G. A review: thermal stability of methylammonium lead halide based perovskite solar cells. *Appl. Sci.* **9**, 188 (2019).
12. Juarez-Perez, E. J. et al. Role of the selective contacts in the performance of lead halide perovskite solar cells. *J. Phys. Chem. Lett.* **5**, 680–685 (2014).
13. Etgar, L. et al. Mesoscopic CH3NH3PbI3/TiO2 heterojunction solar cells. *J. Am. Chem. Soc.* **134**, 17396–17399 (2012).
14. Laban, W. A. & Etgar, L. Depleted hole conductor-free lead halide iodide heterojunction solar cells. *Energy Environ. Sci.* **6**, 3249–3253 (2013).
15. Shi, J. et al. Hole-conductor-free perovskite organic lead iodide heterojunction thin-film solar cells: high efficiency and junction property. *Appl. Phys. Lett.* **104**, 063901 (2014).
16. Eperon, G. E., Burlakov, V. M., Docampo, P., Goriely, A. & Snaith, H. J. Morphological control for high performance, solution-processed planar heterojunction perovskite solar cells. *Adv. Funct. Mater.* **24**, 151–157 (2014).
17. Lin, Z. et al. 2D materials advances: from large scale synthesis and controlled heterostructures to improved characterization techniques, defects and applications. *2D Mater.* **3**, 042001 (2016).
18. Niu, G., Guo, X. & Wang, L. Review of recent progress in chemical stability of perovskite solar cells. *J. Mater. Chem. A* **3**, 8970–8980 (2015).
19. Grätzel, M. The light and shade of perovskite solar cells. *Nat. Mater.* **13**, 838 (2014).
20. Li, X. et al. Outdoor performance and stability under elevated temperatures and long-term light soaking of triple-layer mesoporous perovskite photovoltaics. *Energy Technol.* **3**, 551–555 (2015).
21. Chatterjee, S., Bera, A. & Pal, A. J. p–i–n Heterojunctions with BiFeO3 perovskite nanoparticles and p- and n-type oxides: photovoltaic properties. *ACS Appl. Mater. Inter.* **6**, 20479–20486 (2014).
22. Ye, W., Xiang, J., Huang, F. & Zhong, D. Towards large-area perovskite solar cells: the influence of compact and mesoporous TiO2 electron transport layers. *Mater. Res. Express* **5**, 085506 (2018).
23. Jena, A. K., Numata, Y., Ikegami, M. & Miyasaka, T. Role of spiro-OMeTAD in performance deterioration of perovskite solar cells at high temperature and reuse of the perovskite films to avoid Pb-waste. *J. Mater. Chem. A* **6**, 2219–2230 (2018).
24. Qin, P. et al. Inorganic hole conductor-based lead halide perovskite solar cells with 12.4% conversion efficiency. *Nat. Commun.* **5**, 3834 (2014).
25. Wang, K.-C. et al. Low-temperature sputtered nickel oxide compact thin film as effective electron blocking layer for mesoscopic NiO/CH3NH3PbI3 perovskite heterojunction solar cells. *ACS Appl. Mater. Inter.* **6**, 11851–11858 (2014).
26. Seo, J. et al. Benefits of very thin PCBM and LiF layers for solution-processed p–i–n perovskite solar cells. *Energy Environ. Sci.* **7**, 2642–2646 (2014).
27. Malinkiewicz, O. et al. Metal-oxide-free methylammonium lead iodide perovskite-based solar cells: the influence of organic charge transport layers. *Adv. Energy Mater.* **4**, 1400345 (2014).
28. Wang, B. et al. The charge carrier dynamics, efficiency and stability of two-dimensional material-based perovskite solar cells. *Chem. Soc. Rev.* **48**, 4854–4891 (2019).
29. Capasso, A. et al. Few-layer MoS2 flakes as active buffer layer for stable perovskite solar cells. *Adv. Energy Mater.* **6**, 1600920 (2016).
30. Kakavelakis, G. et al. Extending the continuous operating lifetime of perovskite solar cells with a molybdenum disulfide hole extraction interlayer. *Adv. Energy Mater.* **8**, 1702287 (2018).
31. Najafi, L. et al. MoS2 quantum dot/graphene hybrids for advanced interface engineering of a CH3NH3PbI3 perovskite solar cell with an efficiency of over 20%. *ACS Nano* **12**, 10736–10754 (2018).
32. Singh, E., Kim, K. S., Yeom, G. Y. & Nalwa, H. S. Atomically thin-layered molybdenum disulfide (MoS2) for bulk-heterojunction solar cells. *ACS Appl. Mater. Inter.* **9**, 3223–3245 (2017).
33. Kohnehpoushi, S., Nazari, P., Nejand, B. A. & Eskandari, M. MoS2: a two-dimensional hole-transporting material for high-efficiency, low-cost perovskite solar cells. *Nanotechnology* **29**, 205201 (2018).
34. Akama, T. et al. Schottky solar cell using few-layered transition metal dichalcogenides toward large-scale fabrication of semitransparent and flexible power generator. *Sci. Rep.* **7**, 11967 (2017).
35. Wang, D. et al. MoS2 incorporated hybrid hole transport layer for high performance and stable perovskite solar cells. *Synth. Met.* **246**, 195–203 (2018).
36. Ray, R., Sarkar, A. S. & Pal, S. K. Improving performance and moisture stability of perovskite solar cells through interface engineering with polymer-2D MoS2 nanohybrid. *Sol. Energy* **193**, 95–101 (2019).
37. Coleman, J. N. et al. Two-dimensional nanosheets produced by liquid exfoliation of layered materials. *Science* **331**, 568–571 (2011).
38. O'Neill, A., Khan, U. & Coleman, J. N. Preparation of high concentration dispersions of exfoliated MoS2 with increased flake size. *Chem. Mater.* **24**, 2414–2421 (2012).
39. Giordano, F. et al. Enhanced electronic properties in mesoporous TiO2 via lithium doping for high-efficiency perovskite solar cells. *Nat. Commun.* **7**, 10379 (2016).
40. Radisavljevic, B., Radenovic, A., Brivio, J., Giacometti, V. & Kis, A. Single-layer MoS2 transistors. *Nat. Nanotechnol.* **6**, 147–150 (2011).
41. Gu, X. et al. A solution-processed hole extraction layer made from ultrathin MoS2 nanosheets for efficient organic solar cells. *Adv. Energy Mater.* **3**, 1262–1268 (2013).
42. Huo, N. et al. High carrier mobility in monolayer CVD-grown MoS2 through phonon suppression. *Nanoscale* **10**, 15071–15077 (2018).
43. Dunfield, S. P. et al. From defects to degradation: a mechanistic understanding of degradation in perovskite solar cell devices and modules. *Adv. Energy Mater.* **10**, 1904054 (2020).
44. Habisreutinger, S. N. et al. Carbon nanotube/polymer composites as a highly stable hole collection layer in perovskite solar cells. *Nano Lett.* **14**, 5561–5568 (2014).
45. Abate, A. et al. Protic ionic liquids as p-dopant for organic hole transporting materials and their spplication in high efficiency hybrid solar cells. *J. Am. Chem. Soc.* **135**, 13538–13548 (2013).
46. Abate, A. et al. Lithium salts as "redox active" p-type dopants for organic semiconductors and their impact in solid-state dye-sensitized solar cells. *Phys. Chem. Chem. Phys.* **15**, 2572–2579 (2013).
47. Abate, A., Staff, D. R., Hollman, D. J., Snaith, H. J. & Walker, A. B. Influence of ionizing dopants on charge transport in organic semiconductors. *Phys. Chem. Chem. Phys.* **16**, 1132–1138 (2014).
48. Alfihed, S., Hossain, M., Alharbi, A., Alyamani, A. & Alharbi, F. H. PLD grown polycrystalline tungsten disulphide (WS2) films. *J., Mater.* **2013**, 5 (2013).
49. Hossain, M. I., Alharbi, F. H. & Tabet, N. Copper oxide as inorganic hole transport material for lead halide perovskite based solar cells. *Sol. Energy* **120**, 370–380 (2015).
50. Hossain, M. I., Alharbi, F. H., El-Mellouhi, F. & Tabet, N. Design optimization of solar cell with molybdenum sulfide as light absorber. *J. Photonics Energy* **8**, 1–16 (2018).
51. Hippalgaonkar, K. et al. High thermoelectric power factor in two-dimensional crystals of MoS2. *Phys. Rev. B* **95**, 115407 (2017).
52. Kayyalha, M., Maassen, J., Lundstrom, M., Shi, L. & Chen, Y. P. Gate-tunable and thickness-dependent electronic and thermoelectric transport in few-layer MoS2. *J. Appl. Phys.* **120**, 134305 (2016).

AUTHOR CONTRIBUTIONS

V.N., F.E. and M.L. conceived and designed the study. M.L. and A.A. performed the experiments. M.H. and O.R. are also acknowledged and thanked for the help provided for computational simulation and characterization parts, respectively. A.B. and C.D. are appreciated for the experimental help. ML wrote the paper. V.N., F.E., S.S., N.T., A.B., A.A., M.H. and O.R. reviewed and edited the manuscript. All authors read and approved the manuscript.

COMPETING INTERESTS

The authors declare no competing interests.

ADDITIONAL INFORMATION

Supplementary information is available for this paper at https://doi.org/10.1038/s41699-020-00173-1.

Correspondence and requests for materials should be addressed to M.L., F.E.-M. or V.N.

Reprints and permission information is available at http://www.nature.com/reprints